IOP Publishing Journal of Physics: Condensed Matter
J. Phys.: Condens. Matter **27** (2015) 095302 (8pp) doi:10.1088/0953-8984/27/9/095302

Tunneling through finite graphene superlattices: resonance splitting effect

C Huy Pham[1] **and V Lien Nguyen**[2,3]

[1] SISSA/International School for Advanced Study, Via Bonomea 265, I-34136 Trieste, Italy
[2] Theoretical and Computational Physics Department, Institute of Physics, VAST, 10 Dao Tan, Ba Dinh District, Hanoi 10000, Vietnam
[3] Institute for Bio-Medical Physics, 109A Pasteur, 1st District, Ho Chi Minh City, Vietnam

E-mail: cpham@sissa.it

Received 4 December 2014, revised 16 January 2015
Accepted for publication 26 January 2015
Published 18 February 2015

Abstract

An exact expression of the transmission probability through a finite graphene superlattice with an arbitrary number of potential barriers n is derived in two cases of the periodic potential: rectangular electric potential and δ-function magnetic potential. Obtained transmission probabilities show two types of resonance energy: barrier-induced resonance energies unchanged as n varies and well-induced resonance energies that have undergone the $(n-1)$-fold splitting as n increases. Supported by numerical calculations for various types of graphene superlattices, these analytical findings are assumed to be equally applied to all of the finite graphene superlattices regardless of their potential nature (electric or magnetic) and potential barrier shapes.

Keywords: graphene superlattice, tunneling, resonance splitting

(Some figures may appear in colour only in the online journal)

1. Introduction

Four decades ago, Tsu and Esaki first demonstrated numerically that for a finite semiconductor superlattice with n potential barriers the transmission probability shows the $(n-1)$-fold resonance splitting [1]. Then, this $(n-1)$-fold resonance splitting rule was analytically proved for finite semiconductor superlattices with periodic potentials of arbitrary profile [2, 3]. In the limit of large n, the resonance energies split gradually as n increases, which would eventually form the minibands that are responsible for privileged transport properties of semiconductor superlattices such as the Bloch oscillations or the Stark ladders phenomena [4].

The massless Dirac-like behavior of charge carriers in graphene brings about unusual transport properties of not only pristine graphene itself, but certainly of graphene-based nanostructures [5, 6]. Therefore, graphene superlattices (GSLs), i.e. graphene under periodic potentials, have been extensively studied in a great number of works [7–15] for periodic potentials of a different nature (electric [7–10] or magnetic [11–15]) and different profiles (Kronig–Penney [7, 10, 12, 15], cosine [8] or square [9]). These studies are primarily focused on the behavior of the minibands induced by an infinite periodic potential in the vicinity of the Dirac point and the related transport properties. As for finite GSLs, i.e. graphene-based multi-barrier structures, there are only a few works, where the transmission probability and the conductance are calculated for several values of barrier number n [16–18]. In particular, calculating the transmission probability for the two types of finite magnetic GSLs (with different potential profiles and $n \leqslant 5$), Lu *et al* noticed that the $(n-1)$-fold resonance splitting identified in finite semiconductor superlattices is applied to the finite magnetic GSLs examined [19].

The purpose of this paper is to show that the $(n-1)$-fold resonance splitting mentioned is truly applied to all of the finite GSLs, electric or magnetic, regardless of potential profiles. To this end, using the transfer matrix approach, we have derived an exact expression of the transmission probability across a finite GSL with an arbitrary number of barriers n in two cases of periodic potentials: rectangular electric potential and δ-function magnetic potential. In both cases, obtained transmission probabilities show two types of resonance energy (RE): (i) the barrier-induced REs that

are entirely determined by the single-barrier parameters and completely insensitive to a change in the barrier number n [$n \geqslant 1$] and (ii) the well-induced REs that undergo the $(n-1)$-fold splitting as n increases. These REs could be developed only in the energy ranges corresponding to the minibands in the electronic band of the infinite GSL of the same barrier structure. The analytical findings are fully supported by numerical calculations performed for finite GSLs with periodic potentials of a different nature and shape and, therefore, they are assumed to be equally applied to all of the finite GSLs regardless of potential nature and barrier shape. The most impressive reflection of the resonance behavior of transmission probability, including the $(n-1)$-fold resonance splitting could be found in the conductance which is numerically demonstrated for two types of electric GSLs with rectangular and triangular potential barriers.

The paper is organized as follows. Section 2 is devoted to a systematic study of the transmission probability across electric GSLs that includes (i) to derive an analytical expression of the transmission probability across a finite electric GSL with an arbitrary number of rectangular potential barriers, (ii) to numerically calculate the transmission probability across the finite electric GSLs with different numbers of triangular potential barriers and (iii) to calculate the conductance of the finite electric GSLs examined. Section 3 shows an analytical expression of the transmission probability across a finite magnetic GSL with an arbitrary number of δ-function potential barriers. Results obtained in each section are discussed in detail to identify the resonance spectrum showing the $(n-1)$-fold resonance splitting. The paper concludes with a brief summary in section 4.

2. Electric graphene superlattices

This section is devoted to the finite/infinite GSLs with periodic electric potentials (electric GSLs—EGSLs). We first derive an analytical expression of the transmission probability, T_n, for a finite EGSL with an arbitrary number of rectangular potential barriers, n. The obtained expression shows a full resonance spectrum of T_n, including the $(n-1)$-fold resonance splitting discussed. Then, the resonance properties of T_n found analytically are numerically recognized for one more kind of finite EGSLs—the EGSL with triangular potential barriers. The section concludes by showing the conductances which simply reflect the resonance behavior of the transmission probabilities calculated.

2.1. Analytical expression for EGSLs with rectangular potential barriers

We consider a finite 1D EGSL with n rectangular barriers grown along the x-direction as schematically illustrated in figure 1. We are interested in the case where the low-energy properties of charge carriers in the structure can be described by the massless Dirac-like Hamiltonian

$$H_e = v_F \vec{\sigma}\,\hat{p} + V(x), \tag{1}$$

where $v_F \approx 10^6\,\mathrm{m\,s^{-1}}$ is the Fermi velocity of carriers in pristine graphene, $\vec{\sigma} = (\sigma_x, \sigma_y)$ are the Pauli matrices, $\hat{p} = (p_x, p_y)$ is the in-plane momentum and $V(x)$ describes the periodic potential.

In the simplest case of a single rectangular barrier [$n = 1$], solving the Hamiltonian of equation (1) immediately gives the following expression for the transmission probability [20] (see appendix):

$$T_1 = [\,1 + \sin^2(k_B d_B)[k_y U/\hbar v_F k_W k_B]^2\,]^{-1}, \tag{2}$$

where U is the barrier height, d_B is the barrier width, k_y is the y-component of the wave-vector (which is unaffected by the 1D potential $V(x)$) and $k_{B(W)}$ is the x-component of the wave-vector inside (outside) the barrier region. Given an incident energy E, the wave-numbers $k_{B(W)}$ are defined as

$$k_\lambda = \sqrt{[(E - \eta \cdot U)/\hbar v_F]^2 - k_y^2}\,; \quad \eta = 1 \text{ or } 0 \text{ for } \lambda = B \text{ or } W, \text{ respectively.} \tag{3}$$

The k_y-dependence of T_1 in equation (2) expresses a fundamental difference in transmission behavior between graphene and conventional semiconductors. If $k_y = 0$ the transmission probability T_1 is always equal to unity, regardless of the barrier height as well as the barrier width. This is the so-called Klein tunneling—a relativistic effect observed in graphene.

On the other hand, given a non-zero value of k_y, the transmission probability T_1 of equation (2) varies with the incident energy E and reaches the maximum value of unity at the energies which satisfy the equality $\sin(k_B d_B) = 0$. This equality with k_B defined from equation (3) yields the REs of the transmission probability T_1 for a single rectangular barrier:

$$E_l^{(\pm)} = U \pm \hbar v_F \sqrt{k_y^2 + l^2\pi^2/d_B^2}; \quad l - \text{integers}. \tag{4}$$

For example, figure 1 presents the transmission probability T_1 of equation (2) for the barrier with $U = 8\Gamma$ and $d_B = 5\,\mathrm{nm}$ at $k_y = 0.1\,\mathrm{nm^{-1}}$ ($\Gamma \equiv \hbar v_F/2d_B$, so if $d_B = 5\,\mathrm{nm}$ then $\Gamma \approx 66\,\mathrm{meV}$). The arrows indicate the two REs, $E_1^{(-)}$ and $E_1^{(+)}$, determined from equation (4).

In the opposite limit of large n, an infinite periodic potential produces minibands in the electronic band structure of GSLs. Using the transfer (T) matrix method, it was shown that the electronic band structure problem of infinite EGSLs with rectangular potential barriers is effectively reduced to solving the following transcendental equation for the Bloch wave-number k_x [10, 20]:

$$\cos(k_x d) = f, \tag{5}$$

where

$$f = \cos(k_W d_W)\cos(k_B d_B) + \frac{(U/\hbar v_F)^2 - (k_W^2 + k_B^2)}{2k_W k_B} \times \sin(k_W d_W)\sin(k_B d_B), \tag{6}$$

d_W is the well width and $d = d_B + d_W$ is the superlattice period.

Solutions of equation (5) directly give the electronic band structure that consists of the minibands separated by the

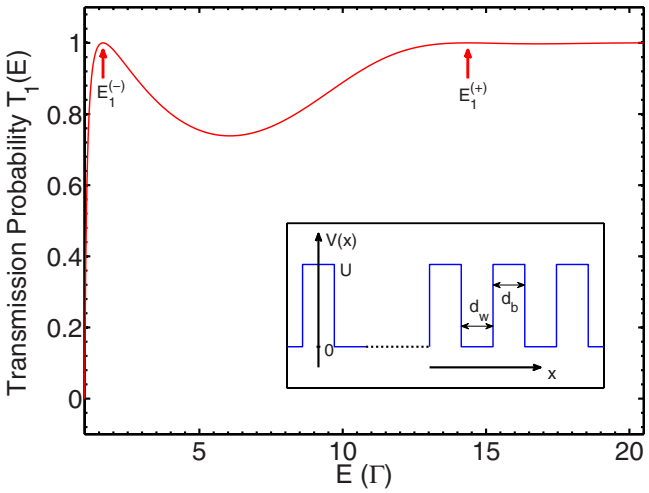

Figure 1. (*a*) Transmission probability T_1 for a single rectangular barrier of $U = 8\Gamma \equiv 8(\hbar v_F/2d_B)$ and $d_B = 5$ nm is plotted versus the incident energy E (for reference: $\Gamma \approx 66$ meV if $d_B = 5$ nm); arrows indicate the REs, $E_1^{(-)}$ and $E_1^{(+)}$, from equation (4); inset: the rectangular potential model under study.

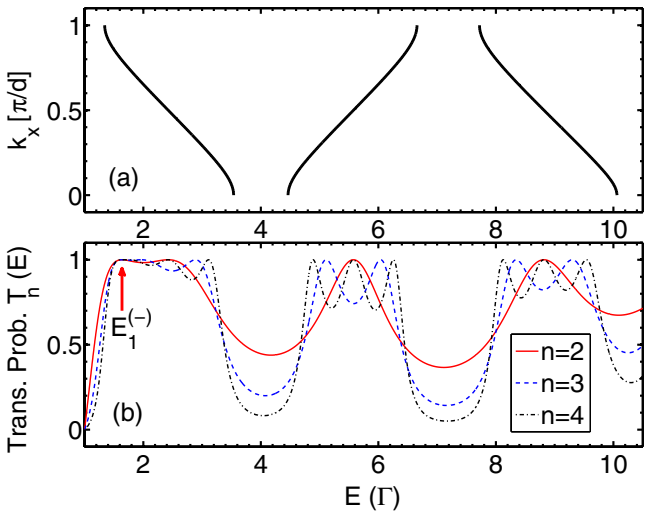

Figure 2. (*a*) Cut of the band structure along the $(k_y = 0.1\,\mathrm{nm}^{-1})$-plane of the infinite EGSL with barrier parameters given in figure 1 and $d_W = d_B$. (*b*) Transmission probability T_n of equation (7) is plotted as a function of the incident energy E for finite EGSLs with different numbers of rectangular barriers n (U and $d_B = d_W$ are the same as in (*a*)); arrow indicates the barrier-induced RE $E_1^{(-)}$ which is completely insensitive to n (energy in units of $\Gamma \equiv \hbar v_F/2d_B$).

band gaps. Figure 2(*a*) shows, for example, the cut of the band structure along the $(k_y = 0.1\,\mathrm{nm}^{-1})$-plane, calculated numerically from equation (5) for the EGSL with the same barrier parameters as in figure 1 and the well width $d_W = d_B$. The solid lines describe the minibands which are separated from each other by the band gaps. Furthermore, once the T-matrix is known one can readily calculate the transmission probability and then the transport characteristics such as the conductance and the shot noise spectrum power [10].

For a finite EGSL with an arbitrary number of rectangular barriers, n, similar to that realized for finite semiconductor superlattices in [2], we are able to obtain an exact expression of the transmission probability (see appendix):

$$T_n = [\,1 + Q^2(k_y U/\hbar v_F k_W k_B)^2 \sin^2(k_B d_B)\,]^{-1}, \quad (7)$$

where

$$Q = \frac{f_+^n - f_-^n}{2\sqrt{f^2-1}} \quad (8)$$

with

$$f_\pm = f \pm \sqrt{f^2-1}, \quad (9)$$

f defined in equation (6) and (the power) n being the number of barriers.

The transmission probability expression of equation (7) is valid for any finite n, including the case of no barrier, $n = 0$, when $T_n \equiv 1$. Particularly, if $n = 1$, the factor Q equals to unity [see equations (8) and (9)] and equation (7) is then reduced to equation (2). Note that the two factors k_y and $\sin^2(k_B d_B)$ are shown at the same place in both T_1 of equation (2) and T_n of equation (7). This implies that the single barrier transmission properties related to these factors, i.e. the Klein tunneling effect and the REs of equation (4), should be equally reserved for all of the finite EGSLs, regardless of the barrier number n. Due to the fact that, given k_y, these REs of equation (4) are determined by only the barrier shape (i.e. U and d_B), they will be hereafter called the barrier-induced REs. However, it should be emphasized that while the barrier-induced REs are reserved for finite EGSLs with an arbitrary number of barriers, n, due to the factor Q^2 in equation (7) the whole resonance spectrum of a finite EGSL should depend on n.

Actually, the factor Q^2 in equation (7) carries all the specific resonance features of the finite EGSLs studied. Regarding the definition of Q in equation (8) we consider two cases of the quantity f. Note here that for a given EGSL and a given incident angle θ, $k_y = k_W \cos\theta$, this quantity is entirely determined by the incident energy E.

In the case of $f^2 > 1$, the equation (5) for infinite EGSLs has no real solution of k_x. This implies a presence of band gaps at the corresponding energies in the electronic band of infinite EGSLs. On the other hand, in this case both quantities $f_\pm$ of equation (9) are real and therefore Q^2 is always positive. The fact that there is nowhere for Q vanished in the ranges of incident energy, corresponding to the condition of $f^2 > 1$, means that all REs which might have emerged in these energy ranges should be those associated with only the factor $\sin^2(k_B d_B)$, i.e. barrier-induced REs (see below).

In the opposite case of $f^2 < 1$, the quantities $f_\pm$ of equation (9) become complex. To search for the Q-behavior in this case, it is convenient to write f in the form $f = \cos\varphi$ with $0 < \varphi < \pi$. Then, from equations (8) and (9) we have

$$Q = \frac{\sin n\varphi}{\sin\varphi}; \quad 0 < \varphi < \pi\,. \quad (10)$$

The transmission probability T_n of equation (7) reaches the maximum of unity at the energies making Q vanished. Certainly, the quantity Q of equation (10) describes well the particular cases of $n = 0$ and $n = 1$ discussed above. For $n = 2$ (double-barrier structure) Q is vanished at the single

energy, corresponding to $\varphi = \pi/2$. That is just the RE of T_2. Since this RE could be developed only in the presence of the well, we will call it the well-induced RE. Increasing the number of barriers/wells, while the barrier-induced REs of equation (4) are firmly unchanged, the well–well correlations cause the well-induced REs split. For a given n, clearly, there are $(n-1)$ values of φ making Q of equation (10) vanished: $\varphi = (m/n)\pi$ with $m = 1, 2, ..., n-1$. Each of these φ-values determines a value of f and further, a RE. Thus, the well-induced RE developed originally in the double-barrier structure becomes split into $(n-1)$ sub-REs as the barrier number n increases. This is just the $(n-1)$-fold resonance splitting claimed in [1, 2, 19]. Here, it should be noted that in the considered case of $f^2 < 1$, the equation (5) has the real solutions which describe minibands in the electronic band of an infinite EGSL. So, we arrive at an important point: the well-induced REs in T_n that can be developed only in the energy ranges corresponding to the minibands in the electronic band of the infinite EGSL with the same periodic potential undergo the $(n-1)$-fold splitting as n increases.

Concerning the location of barrier-induced REs, note that the condition which determines these REs, $\sin^2(k_B d_B) = 0$, converts the quantity f of equation (6) into $f = \cos(k_W d_W)\cos(k_B d_B)$ with $f^2 < 1$. This means that, like well-induced REs, barrier-induced REs could be developed only in the energy ranges corresponding to the minibands in the electronic band of the related infinite EGSL.

Thus, equation (7) describes fully the transmission properties of finite EGSLs with rectangular potential barriers. It seems that there are two types of REs (where the transmission becomes perfect): (i) barrier-induced REs that are entirely determined by the single barrier parameters and are the same for all finite EGSLs, regardless of barrier number n and (ii) well-induced REs that undergo the $(n-1)$-fold splitting as n increases. All of the REs could be developed only in the energy ranges corresponding to the minibands in the band structure of the related infinite EGSL. As a demonstration of these statements we show in figure 2(b) the transmission probability T_n of equation (7) plotted as a function of the incident energy E for finite EGSLs with a different number of rectangular barriers, n. Clearly, (i) all of the REs appeared in the energy ranges corresponding to the minibands in figure 2(a), (ii) the barrier-induced RE ($E_1^{(-)}$ indicated by the arrow) is the same for all finite EGSLs examined and (iii) the well-induced REs undergo the $(n-1)$-fold splitting as the barrier number n increases (see the peaks in the energy ranges of ≈(1.5–3.5), (4.5–6.5) and (7.8–9.8 Γ) in figure 2(b)). Note that the barrier-induced REs may share the place with well-induced REs in a narrow energy range, depending on k_y (see the energy range of (1.5–3.5 Γ) in figure 2(b)). Such a coexistence of both types of REs might lead to a mistake in observing the $(n-1)$-fold resonance splitting effect.

2.2. Numerical demonstrations for EGSLs with triangular potential barriers

For periodic potential barriers other than rectangular ones, the T_n-expressions similar to equation (7) could be derived in the same way as the T-matrix method as realized above (see the magnetic GSL in the next section as an example). Here, we limit ourselves to presenting numerical calculations for one more electric potential barrier model—the one-dimensional triangular barriers illustrated in figure 3. In this model, for a single lattice unit, $0 \leqslant x \leqslant d$, the potential $V(x)$ in the Hamiltonian of equation (1) takes the form $V(x) = (U/d)x$, where U and d are barrier height and superlattice period, respectively. Note that in this potential model a multi-barrier structure (finite EGSL) is characterized by the three parameters: U, d and the barrier number n.

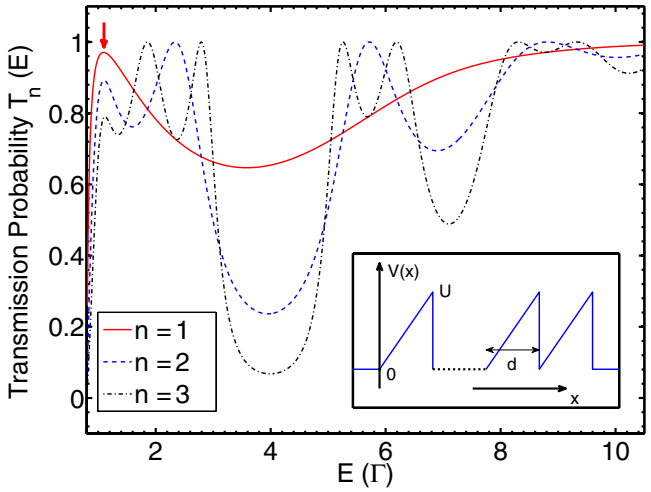

Figure 3. Transmission probability T_n as a function of the incident energy E: numerical calculations for finite EGSLs with different numbers of triangular barriers n ($U = 8\Gamma \equiv 8(\hbar v_F/d)$ and $d = 8$ nm); arrow indicates the barrier-induced RE which is insensitive to n (note: at this energy the transmission is imperfect and the resonance peaks become lower as n increases). Inset: the triangular potential barrier model under study.

In general, the transmission probability across any multi-barrier structure of periodic potentials can be numerically calculated by means of the T-matrix as suggested in [21]. We have in this way calculated the transmission probability T_n for finite EGSLs with a different number of triangular barriers, n[4]. Results shown in figure 3 are for the barriers of $U = 8\Gamma$ and $d = 8$ nm at $k_y = 0.1\,\text{nm}^{-1}$ ($\Gamma \equiv \hbar v_F/d$). On the one hand, the resonance spectrum of T_n in this figure is rather similar to that in figure 2(b). The $(n-1)$-fold splitting of well-induced REs is clearly recognized (see the peaks in the energy ranges of ≈(1.6–3.2), (4.8–6.6) and (7.8–9.8 Γ)). These energy ranges are believed to be corresponding to the minibands in the electronic band of the infinite EGSL with the same periodic potential (by checking the band structure similar to figure 2(a)).

On the other hand, there is an important difference between figure 3 (for triangular barriers) and figure 2(b) (for rectangular barriers) in relation to the 'barrier-induced' REs. At these energies, all of T_n are equal to unity in figure 2(b) (perfect transmission), while figure 3 shows $T_1 < 1$ and even T_n

[4] In T-matrix numerical calculations the problem of instability may be encountered in relation to the terms of $\exp(\pm ikd)$ when k is imaginary and d is large (see appendix A). Such the numerical instability is not appeared in the present calculations with parameters chosen appropriately.

decreasing as n increases (enhanced imperfect transmission). Such an imperfect transmission at the barrier-induced REs observed in figure 3 is first related to a smoothness of the triangular potential that partly prevents the Klein tunneling across the barrier. In addition, this smooth potential effect should be accumulated with increasing barrier number that makes T_n decrease as n increases. Such T_n-behavior at the barrier-induced REs identified in figure 3 for finite EGSLs with triangular potential barriers should be observed in the resonance spectrum of any finite EGSL with smooth potential barriers.

It is worth mentioning that we have carried out numerical calculations of $T_n(E)$ for finite EGSLs in the potential models other than those considered above. The obtained results are all similar to figure 3 in supporting the presence of two types of REs as deduced from equation (7). The $(n-1)$-fold resonance splitting is the property of (only) the well-induced REs and should be observed in the resonance spectrum of any finite EGSL, regardless of the potential barrier profile.

2.3. Conductance

An accurate reflection of the resonance behavior of transmission probability could be found in the conductance. Given the transmission probability $T(E,\theta)$, the conductance at zero temperature can be calculated within the Landauer formalism:

$$G = G_0 \int_{-\pi/2}^{\pi/2} T(E,\theta)\cos\theta \mathrm{d}\theta, \qquad (11)$$

where $G_0 = 4e^2 E_F W/\hbar^2 v_F$, E_F is Fermi energy and W is the sample size along the y-direction. Using equation (11) the conductance G has been calculated for two types of finite EGSLs with T_n given in figures 2 (rectangular barriers) and 3 (triangular barriers). The obtained results are presented in figure 4.

In both figures 4(a) and (b) all three curves of different n reach their highest peaks at the energy close to the barrier-induced RE ($\approx$1.6 Γ in (a) and $\approx$1.1 Γ in (b)). For the rectangular barriers in figure 4(a) all three peaks at this energy are equal in height, independent of the barrier number n. For the triangular barriers in figure 4(b), however, in consistency with the transmission probabilities in figure 3 these peaks are lowered as n increases.

Importantly, beyond the highest peak at the barrier-induced RE the peaks in $G(E)$-curves at higher energies in both figures 4(a) and (b) reflect well the $(n-1)$-fold resonance splitting found in the transmission probability (again, due to a smoothness of triangular barriers this splitting is less clear in figure 4(b) compared to figure 4(a) for sharp barriers of rectangular profile).

3. Magnetic graphene superlattices

Now, we consider the GSLs with periodic magnetic potential barriers (magnetic GSLs—MGSLs). The $(n-1)$-fold

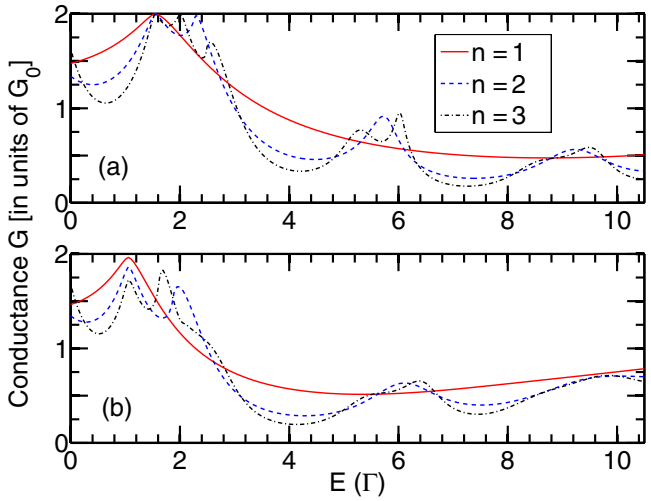

Figure 4. Conductance G (in units of G_0) is plotted as a function of the incident energy E (in units of Γ) for the finite EGSLs with different numbers of rectangular potential barriers (a) (T_n given in figure 2) or triangular potential barriers (b) (T_n given in figure 3). The $G(E)$-dependence adequately reflects the resonance behavior of $T_n(E)$.

resonance splitting was numerically demonstrated for two types of MGSLs with step and sinusoidal barriers [19]. Actually, there is a close relation in electronic properties between corresponding EGSLs and MGSLs [22]. So, certainly, it is possible to derive analytical expressions of the transmission probability for the finite MGSLs in the same way as that realized above for the EGSLs.

Indeed, for definition, we consider the case of δ-function magnetic barriers as schematically illustrated in figure 5. The magnetic field is assumed to be uniform in the y-direction and staggered as periodic δ-function barriers of alternative signs in the x-direction, so for a single lattice unit the field profile has the form

$$\vec{B} = B_0[\delta(x + d_B/2) - \delta(x - d_B/2)]\,\hat{z},$$

where B_0 is the barrier strength and d_B is the barrier width. The corresponding vector potential $\vec{A}$ in the Landau gauge is

$$\vec{A}(x) = B_0 l_B \Theta(d_B/2 - |x|)\,\hat{y},$$

where $\Theta(x)$ is the Heaviside step function and $l_B = \sqrt{\hbar c/eB_0}$ is the magnetic length. Due to a richness of fundamental electronic properties and a simplicity of mathematical treatment the infinite MGSLs with these δ-function barriers have been extensively studied [11, 15, 17]. The possibility of realizing multiple δ-function magnetic barriers in experiments has been discussed in detail in [17].

In the case of MGSLs with the vector potential $\vec{A}$, instead of H_e of equation (1) we have to deal with the Hamiltonian of the form

$$H_m = v_F\vec{\sigma}(\hat{p} + e\vec{A}),$$

where e is the elementary charge. It seems that the transmission probability T_n for the finite MGSLs described by this Hamiltonian can be derived in exactly the same way as

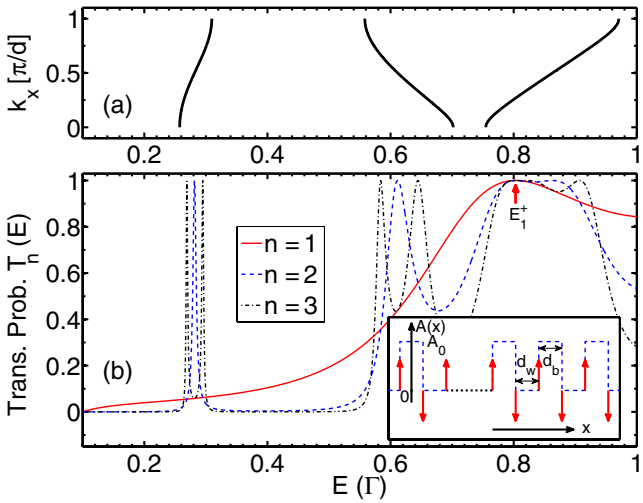

Figure 5. (*a*) Cut of the band structure along the ($k_y = 0.1\,\mathrm{nm}^{-1}$)-plane of the infinite MGSL with $A_0 = 0.4$, $d_B = d_W = 5\,\mathrm{nm}$. (*b*) Transmission probability T_n of equation (14) is plotted as a function of the incident energy E for finite MGSLs with different numbers of δ-function barriers n ($A_0 = 0.4$, $d_B = d_W = 5\,\mathrm{nm}$); arrow indicates the barrier-induced RE $E_1^{(+)}$ which is insensitive to n. Inset: the δ-function magnetic potential barrier model under study.

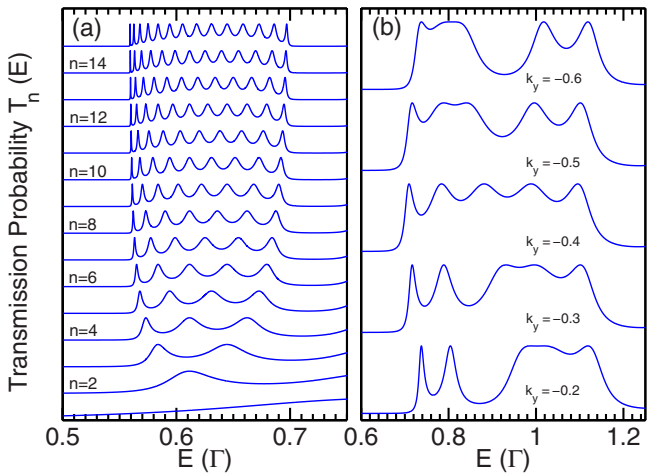

Figure 6. (*a*) The $(n-1)$-fold resonance splitting is demonstrated in more detail in a narrow energy range from figure 5, but n is now up to 15. (*b*) To demonstrate the k_y-dependence of the resonance spectrum of transmission probability: $T_3(E)$ for the same finite MGSL with δ-function potential barriers ($A_0 = 0.8$, $d_B = d_W = 5\,\mathrm{nm}$ and $n = 3$) in the same energy range, but at different k_y-values in units of nm^{-1} (given in the figure).

that realized above for EGSLs. So, it is reasonable to mention only the differences between the two problems.

The transmission probability for a single δ-function magnetic barrier takes the form

$$T_1 \;=\; [\,1+\sin^2(k_B d_B)[eA_0E/\hbar^2 v_F k_W k_B]^2\,]^{-1}, \qquad (12)$$

where

$$k_\lambda \;=\; \sqrt{(E/\hbar v_F)^2-(k_y+\eta\cdot eA_0/\hbar)^2}\;;\quad \eta = 1 \;\text{ or }\; 0$$
$$\text{for } \lambda = B \;\text{ or }\; W, \;\text{ respectively.}$$

These expressions are respectively in place of equations (3) and (4) in the case of EGSLs. Note that different from equation (3) there is no k_y-factor in the second term in T_1 of equation (12). So, the transmission probability through a single δ-function magnetic barrier might be finite even at $k_y = 0$ (The k_y-dependence of T_1 (12) is numerically demonstrated in [17]).

The transmission probability T_1 of equation (12) shows the REs

$$E_l^{(\pm)} \;=\; \pm\hbar v_F\sqrt{(k_y+eA_0/\hbar)^2+l^2\pi^2/d_B^2};\;\; l-\text{integers},$$

which are similar to REs of equation (4) determined entirely by the single barrier parameters (barrier-induced REs).

The transcendental equation of equation (5) is equally applied for the δ-function magnetic barriers, but the quantity f of equation (6) is now replaced by

$$f \;=\; \cos(k_W d_W)\cos(k_B d_B) - \frac{(eA_0/\hbar)^2+(k_W^2+k_B^2)}{2k_W k_B} \times \sin(k_W d_W)\sin(k_B d_B). \qquad (13)$$

The only difference between the two quantities f in equation (6) (for electric rectangular barriers) and equation (13) (for δ-function magnetic barriers) is that the product $k_y U$ in equation (6) is replaced by $eA_0E/\hbar$ in equation (13).

Furthermore, the transmission probability through a finite MGSL with an arbitrary number of δ-function barriers can be obtained in the form

$$T_n \;=\; [\,1+Q^2(eA_0E/\hbar^2 v_F k_W k_B)^2\sin^2(k_B d_B)\,]^{-1}. \qquad (14)$$

The rest of the expressions of Q and $f_\pm$, equations (8) and (9), are the same for both EGSL and MGSL problems under study.

It is important to note that while the transmission probabilities T_n of equations (7) and (14) are very different in the k_y-dependence, all the factors related to the REs in these two T_n-expressions are exactly the same (i.e. $\sin^2(k_B d_B)$ and Q^2). So, everything we have stated about the resonance spectrum of finite EGSLs in the previous section, including the $(n-1)$-fold splitting of the well-induced REs, is undoubtedly reserved for the finite MGSLs considered.

As a demonstration, we present in figure 5(*b*) the transmission probability T_n of equation (14) plotted versus the incident energy E for finite MGSLs with different numbers of δ-function barriers ($A_0 = 0.4$ and $d_B = d_W = 5\,\mathrm{nm}$). Figure 5(*a*) shows the miniband structure of the corresponding infinite MGSL. Clearly, like figures 2 and 3 for finite EGSLs, figure 5(*b*) shows (i) the barrier-induced REs $E_1^{(+)}$ (indicated by the arrow) that are the same ($\approx 0.8\,\Gamma$) for all the MGSLs with different n and (ii) the well-induced REs that undergo the $(n-1)$-fold splitting. These REs are all emerged in the range of energy corresponding to minibands in figure 5(*a*).

In order to see the resonance spectrum in a large range of energy all the figures 2, 3 and 5 are limited to some small values of n. In addition, figure 6(*a*) is focused on showing in more detail the $(n-1)$-fold resonance splitting in a narrow energy range, $\approx$0.5–0.7 Γ, separated from figure 5. In this narrow energy range it is possible to distinguish the well-induced resonance peaks even if n is relatively large. Figure 6(*a*) is a typical demonstration of the $(n-1)$-fold resonance splitting

in which we are interested. Similar pictures could certainly be set in other energy ranges and for various types of MGSLs as well as EGSLs.

Finally, we would like to note that besides the structural parameters U, d_B, d_W and n, the resonance spectrum of a finite GSL depends on the k_y-value. This can be seen, for example, in figure 6(b), where the transmission probabilities are shown in the same energy range for the same finite MGSL with $A_0 = 0.8$, $d_B = d_W = 5$ nm and $n = 3$, but at different values of k_y. This figure obviously demonstrates a strong and unsystematic k_y-dependence of the position as well as the half-width of resonance peaks. Due to this k_y-dependence, an appropriate k_y-value should be chosen to gain a clear picture of the $(n-1)$-fold resonance splitting.

4. Conclusions

We have systematically studied the resonance spectrum of the transmission probability through finite EGSLs and MGSLs with different potential barrier shapes. For the finite EGSL with rectangular potential barriers and the finite MGSL with δ-function potential barriers the transmission probability $T_n(E)$ has been derived analytically. The obtained $T_n(E)$-expressions show two types of REs, barrier-induced and well-induced. The barrier-induced REs are entirely determined by the single-barrier parameters (given k_y) and remain unchanged as the barrier number n varies [$n \geqslant 1$]. The well-induced REs undergo the $(n-1)$-fold splitting as the barrier number n increases. These REs of T_n all emerged in the energy range corresponding to the minibands in the electronic band of the related infinite GSL.

The analytical findings are fully supported by numerical calculations carried out for finite EGSLs/MGSLs with different potential barrier shapes. So, it is reasonable to assume that they should be equally applied to all of the finite GSLs, regardless of potential nature (electric or magnetic) and potential barrier shape. Although the $(n-1)$-fold resonance splitting found in the present work is the same as that claimed before in [1, 3, 19], it is worth emphasizing that this splitting is only associated with the well-induced REs. Actually, a typical reflection of the resonance behavior of transmission probabilities T_n, including the $(n-1)$-fold splitting of the well-induced REs, can be found in the conductance.

In fact, the GLSs considered in the present work are the single-layer graphene-based superlattices. For the finite bilayer-graphene-based superlattices we are only able to calculate T_n numerically. Remarkably, numerical calculations performed for two potential models, the electric potential studied in [23] and the magnetic potential studied in [24], show seemingly the $(n-1)$-fold resonance splitting similar to that presented above for single-layer graphene superlattices.

Acknowledgments

This work was financially supported by the Vietnam National Foundation for Science and Technology Development under Grant No. 103.02-2013.17.

Appendix

Since the transmission probability T can be exactly expressed in terms of $\mathcal{T}$-matrix elements,

$$T = 1 - \frac{|\mathcal{T}_{21}|^2}{|\mathcal{T}_{22}|^2}, \tag{A.1}$$

to find T for a structure we should calculate the corresponding $\mathcal{T}$-matrix.

(a) *Transmission probability T_1 of equation (2).* In the case of constant potential, $V(x) = V_n = $ constant, the wavefunctions of the Hamiltonian of equation (1) can be found in the form $\Psi(x, y) = M_n R_n(x) C_n \exp(\mathrm{i}k_y y)$ [21], where

$$M_n = \begin{pmatrix} 1 & 1 \\ \frac{\hbar v_F(k_n + \mathrm{i}k_y)}{E - V_n} & \frac{\hbar v_F(-k_n + \mathrm{i}k_y)}{E - V_n} \end{pmatrix}, \tag{A.2}$$

$$R_n = \mathrm{diag}\left[\mathrm{e}^{\mathrm{i}k_n x}, \mathrm{e}^{-\mathrm{i}k_n x}\right], \tag{A.3}$$

$k_n = \sqrt{[(E - V_n)/\hbar v_F]^2 - k_y^2}$ and $C_n = (A_n, B_n)^T$ being the wavefunction amplitude.

So, in solving the Hamiltonian of equation (1) for the single rectangular potential defined as

$$V(x) = \begin{cases} U & \text{if } x_0 \leqslant x \leqslant x_0 + d_B, \\ 0 & \text{otherwise,} \end{cases}$$

the continuity of the wavefunctions at $x = x_0$ and $x = x_0 + d_B$ reads:

$$M_W R_W(x_0) C_1 = M_B R_B(x_0) C_2$$
$$M_B R_B(x_0 + d_B) C_2 = M_W R_W(x_0 + d_B) C_3.$$

Here, C_1, C_2 and C_3 are respectively the amplitudes of wavefunctions in the left, inside and the right of the barrier; $M_{W(B)}$ and $R_{W(B)}$ are respectively defined in equations (A.2) and (A.3) for $V_n = 0(U)$.

From the $\mathcal{T}$-matrix relation, $C_3 = \mathcal{T} C_1$, the $\mathcal{T}$-matrix for the single barrier considered can be obtained as

$$\mathcal{T}(x_0) = R_W^{-1}(x_0 + d_B) M_W^{-1} M_B R_B(d_B) M_B^{-1} M_W R_W(x_0).$$

Regarding the expression of equation (A.1), this $\mathcal{T}$-matrix immediately gives the transmission probability T_1 of equation (2). Here, note that T_1 doesn't depend on x_0 as it should.

The matrix $\mathcal{T}(x_0)$ has an important property

$$\mathcal{T}(x_0) = R_W^{-1}(x_0) \mathcal{T}(0) R_W(x_0), \tag{A.4}$$

which is useful for calculating the $\mathcal{T}$-matrix for a multi-barrier structure.

(b) *Transmission probability T_n of equation (7).* For a finite EGSL with n rectangular barriers the potential $V(x)$ in the Hamiltonian of equation (1) has the form

$$V(x) = \begin{cases} U & \text{if } (j-1)d \leqslant x \leqslant (j-1)d + d_B, \\ 0 & \text{otherwise,} \end{cases}$$

where j is an integer, $1 \leqslant j \leqslant n$, U, d_B and d are defined above.

Actually, the $\mathcal{T}$-matrix for this multi-barrier potential can be calculated as

$$\mathcal{T}_n = \mathcal{T}(nd)...\mathcal{T}(2d)\mathcal{T}(d)\mathcal{T}(0). \quad \text{(A.5)}$$

Using equation (A.4), we write $\mathcal{T}_n = R_W^{-n}(d)[R_W(d)\mathcal{T}(0)]^n$, where the matrix $P(d) \equiv R_W(d)\mathcal{T}(0)$ is often called a characteristic matrix. It could be shown that [17]

$$[P(d)]^n = \begin{pmatrix} p_{11}Q_n - Q_{n-1} & p_{12}Q_n, \\ p_{21}Q_n & p_{22}Q_n - Q_{n-1} \end{pmatrix},$$

where Q_n is given in equation (8) and p_{ij} $(i, j = 1, 2)$ are components of the matrix $P(d)$.

Using the $\mathcal{T}_n$-matrix of equation (A.5), some lengthy, but elementary algebraic calculations give the transmission probability of equation (7).

References

[1] Tsu R and Esaki L 1973 *Appl. Phys. Lett.* **22** 562
[2] Liu X-W and Stamp A P 1993 *Phys. Rev.* B **47** 16605
[3] Liu X-W and Stamp A P 1994 *Phys. Rev.* B **50** 1588
[4] Esaki L and Tsu R 1970 *IBM J. Res. Dev.* **14** 61
[5] Castro Neto A H, Guinea F, Peres N M R, Novoselov K S and Geim A K 2009 *Rev. Mod. Phys.* **81** 109
[6] Das Sarma S, Adam S, Hwang E H and Rossi E 2011 *Rev. Mod. Phys.* **83** 407
[7] Park C-H, Yang L, Son Y-W, Cohen M L and Louie S G 2008 *Nat. Phys.* **4** 213
Park C-H, Yang L, Son Y-W, Cohen M L and Louie S G 2009 *Phys. Rev. Lett.* **101** 126804
Park C-H, Yang L, Son Y-W, Cohen M L and Louie S G 2009 *Phys. Rev. Lett.* **103** 046808
[8] Brey L and Fertig H A 2009 *Phys. Rev. Lett.* **103** 046809
[9] Barbier M, Vasilopoulos P and Peeters F M 2010 *Phys. Rev.* B **81** 075438
[10] Pham C H, Nguyen H C and Nguyen V L 2010 *J. Phys.: Condens. Matter* **22** 425501
[11] Ghosh S and Sharma M 2009 *J. Phys.: Condens. Matter* **21** 292204
[12] Masir M R, Vasilopoulos P and Peeters F M 2010 *J. Phys.: Condens. Matter* **22** 465302
[13] Snyman I 2009 *Phys. Rev.* B **80** 054303
[14] Dell' Anna L and De Martino A 2011 *Phys. Rev.* B **83** 155449
[15] Le V Q, Pham C H and Nguyen V L 2012 *J. Phys.: Condens. Matter* **24** 345502
[16] Bai C and Zhang X 2007 *Phys. Rev.* B **76** 075430
[17] Masir M R, Vasilopoulos P and Peeters F M 2009 *New J. Phys.* **11** 095009
[18] Barbier M, Vasilopoulos P, Peeters F M and Pereira J M Jr 2009 *Phys. Rev.* B **79** 155402
[19] Lu W-T, Li W, Wang Y-L, Ye C-Z and Jiang H 2012 *J. Appl. Phys.* **112** 083712
[20] Barbier M, Peeters F M, Vasilopoulos P and Pereira J M Jr 2008 *Phys. Rev.* B **77** 115446
[21] Nguyen H C and Nguyen V L 2009 *J. Phys.: Condens. Matter* **21** 045305
[22] Tan L Z, Park C-H and Louie S G 2010 *Phys. Rev.* B **81** 195426
[23] Pham C H and Nguyen V L 2014 *J. Phys.: Condens. Matter* **26** 425502
[24] Pham C H, Nguyen T T and Nguyen V L 2014 *J. Appl. Phys.* **116** 123707